Pseudoentanglement of Spin States in the Multilevel $^{15}N@C_{60}$ System

M. Mehring,[1] W. Scherer,[1] and A. Weidinger[2]
[1]*Physikalisches Institut, Universität Stuttgart, D-70550 Stuttgart, Germany*
[2]*Hahn-Meitner-Institut Berlin, D-14109 Berlin, Germany*
(Received 28 March 2004; published 11 November 2004)

We have prepared combined electron and nuclear spin pseudoentangled states $\Psi_{27}^{\pm}$ and $\Phi_{18}^{\pm}$ out of the total number of eight quantum states in the multilevel quantum system of a nitrogen atom with electron spin 3/2 and nuclear spin 1/2 encaged in the endohedral fullerene $^{15}N@C_{60}$. Density matrix tomography was applied to verify the degree of entanglement.

DOI: 10.1103/PhysRevLett.93.206603 PACS numbers: 72.80.Rj, 03.65.Ud, 03.67.–a, 76.30.–v

Entanglement of quantum states is at the heart of quantum physics. It was one of the most intensely debated principles of quantum mechanics from its beginning [1]. A renaissance of quantum mechanics has begun recently with the proposal of quantum information processing [2]. Here entanglement is one of the key ingredients which allows superior performance as compared with classical information processing. Entanglement is an issue not only in quantum cryptography but also in quantum computing. The preparation and detection of entangled quantum states is therefore of central importance in this rapidly developing area of science. The basic unit of a quantum computer is the quantum bit (qubit) with two quantum states. Coupling between several qubits allows one to entangle their quantum states, corresponding to a new state of quantum correlation. Entanglement of nonspin quantum states has been demonstrated with photons [3,4] and ions in an ion trap [5].

Here we are dealing with a ^{15}N atom encaged in C_{60}, an almost spherical surrounding leading to very narrow lines, even in the solid state, which allows precise control of the quantum states. The sample was prepared by ion bombardment of C_{60} with ^{15}N ions followed by chromatographic separation as described in [6] resulting in a concentration of $\approx 10^{-4}$ $^{15}N@C_{60}$ molecules in solid C_{60}. Its endohedral character was established by ESR and electron-nuclear double resonance (ENDOR) measurements [6,7]. Except for the ^{15}N atoms and the 1.1% naturally abundant ^{13}C atoms there are no further magnetic elements in the system. The sample size used here amounts to a few mg. The experiments were performed at *X*-band (9.5 GHz) frequencies at a temperature of 50 K.

There have been proposals to use $^{15}N@C_{60}$ as a qubit in quantum computers [8–10]. In this contribution we demonstrate that $^{15}N@C_{60}$ can be considered, in fact, a basic processing unit in a quantum processing machine provided one selects the appropriate quantum states. In particular, we point at the multilevel nature of the spin states in $^{15}N@C_{60}$ from which we attempt to prepare a two-qubit subspace which might be suitable as a basic quantum machine. We discuss different versions of entanglement and detail the detection of these entangled states. Although we are dealing with an ensemble of these quantum states at a temperature above the quantum limit, we believe that the procedures demonstrated here can be applied to a pure quantum system with similar results as is discussed in the following.

We have presented recently a scheme for creating entangled states between an electron spin 1/2 and a nuclear spin 1/2 in a solid [11]. Because of the rather large inhomogeneous linewidth, only the principle could be demonstrated with only an estimate of the degree of entanglement based on some stringent assumptions. The situation of $^{15}N@C_{60}$ is quite different, not only because of the much higher degree of isolation of the spin system from the surrounding with much longer decoherence time, but also, more importantly, because of its multilevel structure which is more akin to the situation encountered in ion- and atom-quantum computers.

In ensemble quantum computing, which has been demonstrated already extensively in liquid state nuclear magnetic resonance (NMR) [12–16], a large number of elementary quantum computers work in parallel. At elevated temperatures the total density matrix which represents the quantum states is in a mixed state. This has some fundamental consequences as was pointed out early by Warren *et al.* [17]. It became obvious from the work of Cory *et al.* [12,18], Gershenfeld and Chuang [19], and Knill *et al.* [20] that the corresponding quantum states can be viewed as *pseudopure* quantum states.

The entanglement of spin states is usually referred to two spins 1/2. However, here we present an experimental investigation in which an electron spin $S = 3/2$ with the four quantum states $|+3/2\rangle, |+1/2\rangle, |-1/2\rangle, |-3/2\rangle$ is entangled with the two states $|\pm 1/2\rangle$ of the ^{15}N nuclear spin $I = 1/2$. This is quite unusual and leads to

 © 2004 The American Physical Society

interesting consequences. The corresponding Hamiltonian for the electron spin $S = 3/2$ and nuclear spin $I = 1/2$ of $^{15}N@C_{60}$ is in first order given by $\mathcal{H} = \hbar(\omega_S S_z + \omega_I I_z + a S_z I_z)$ with energy eigenvalues $E(m_s, m_I) = \hbar(\omega_S m_S + \omega_I m_I + a m_S m_I)$, where a is the ^{15}N hyperfine interaction and ω_S and ω_I are the corresponding Larmor frequencies of the electron and the nuclear spin. The eigenstates $|m_S m_I\rangle$ are labeled here by numbers $\{|1\rangle, |2\rangle, \cdots, |8\rangle\}$ which correspond to the states $\{|\frac{3}{2}\,\frac{1}{2}\rangle, |\frac{3}{2}\,-\frac{1}{2}\rangle, \cdots, |-\frac{3}{2}\,-\frac{1}{2}\rangle\}$. The related level diagram is shown in Fig. 1.

The states numbered $|1\rangle \cdots |8\rangle$ in Fig. 1 represent all possible quantum states $|m_S m_I\rangle$ where the dominant level splitting results from the Larmor frequency of the electron spin. Vertical transitions ($\Delta m_S = \pm 1$) correspond to ESR transitions at GHz frequencies, whereas horizontal transitions ($\Delta m_I = \pm 1$) correspond to NMR transitions at MHz frequencies. This leads to two ESR lines, separated by $a_{15} = -22.08$ MHz and four NMR lines at frequencies 31.70 MHz ($m_S = 3/2$), 34.55 MHz ($m_S = -3/2$), 9.67 MHz ($m_S = 1/2$), and 12.41 MHz ($m_S = -1/2$).

Before discussing the entangled states in this system we recall that for two spins 1/2 the four Bell states,

$$\Psi^{(\pm)} = \frac{1}{\sqrt{2}}(|+-\rangle \pm |-+\rangle), \tag{1}$$

$$\Phi^{(\pm)} = \frac{1}{\sqrt{2}}(|++\rangle \pm |--\rangle), \tag{2}$$

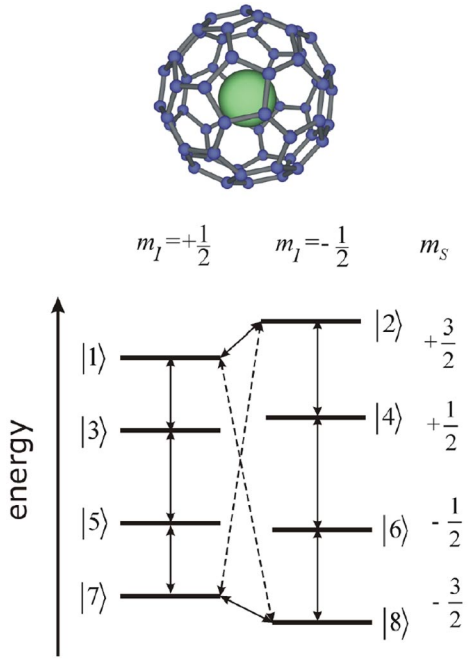

FIG. 1 (color online). Level diagram of the eight spin states of $^{15}N@C_{60}$. Allowed transitions (solid lines) and forbidden transitions between selected entangled states (dashed lines) are indicated.

comprise all possible entangled states. Here we use the shorthand notation $|\pm\pm\rangle$ for $|\pm\frac{1}{2}\pm\frac{1}{2}\rangle$. The $^{15}N@C_{60}$ system allows for the following 24 two-qubit entangled states of the type $\psi_{jk}^{\pm} = \frac{1}{\sqrt{2}}(|j\rangle \pm |k\rangle)$ with $jk \in \{14, 23, 36, 45, 58, 67, 16, 25, 38, 47, 18, 27\}$. In this contribution we restrict ourselves to the preparation of the two special cases

$$\Psi_{27}^{\pm} = \frac{1}{\sqrt{2}}(|2\rangle \pm |7\rangle) = \frac{1}{\sqrt{2}}\left(\left|+\frac{3}{2}-\frac{1}{2}\right\rangle \pm \left|-\frac{3}{2}+\frac{1}{2}\right\rangle\right), \tag{3}$$

$$\Phi_{18}^{\pm} = \frac{1}{\sqrt{2}}(|1\rangle \pm |8\rangle) = \frac{1}{\sqrt{2}}\left(\left|+\frac{3}{2}+\frac{1}{2}\right\rangle \pm \left|-\frac{3}{2}-\frac{1}{2}\right\rangle\right), \tag{4}$$

out of the many possible two-qubit entangled states. Except for the quantum number 3/2 in the $|\pm\frac{3}{2}\rangle$ electronic spin states, these four entangled states are equivalent to the Bell states. In the following we consider the $|\pm\frac{3}{2}\rangle$ states of the electron spin as a qubit and the nuclear spin I as the second qubit. Correspondingly the four quantum states $|\pm\frac{3}{2}\pm\frac{1}{2}\rangle$ define our two-qubit subsystem referred to in the following as $|\pm\pm\rangle$.

The initial Boltzmann density matrix represents a highly mixed state at our environmental parameters. Invoking the pseudopure density matrix concept, we start from the truncated initial Boltzmann density matrix $-S_z/2$ and add a constant term later. Appropriate microwave and radio frequency pulses are applied to create a pseudopure density matrix first. We use the definitions $P_y^{(\pm)}(\beta)$ for pulses applied at electron spin transitions and $P_y^{(jk)}(\alpha)$ for pulses at nuclear spin transitions $(jk) = |j\rangle \leftrightarrow |k\rangle$ in the y direction of the corresponding rotating frames.

In order to generate pseudopure initial density matrices and entangled states of the sublevel set 1, 2, 7, 8, we have applied transition selective ESR and ENDOR pulses. For the entangled states $\Psi_{27}^{\pm}$ we require an initial density matrix $\rho_7 = |7\rangle\langle 7|$, whereas for $\Phi_{18}^{\pm}$ we start from $\rho_8 = |8\rangle\langle 8|$. Let us consider the initial density matrix $\rho_7 = |7\rangle\langle 7|$ which corresponds to $\rho_{(-+)} = |-+\rangle\langle -+|$ in the four level subsystem. It was prepared by applying $P_y^{(-)}(\beta_0)$ with $\beta_0 = \arccos(-1/3)$ to the Boltzmann state, followed after a waiting time to let off-diagonal states decay, by the pulse $P_y^{(12)}(\pi/2)$. After another waiting time of 100 μs the wanted pseudopure state is reached.

The population difference of the $|\frac{3}{2}\pm\frac{1}{2}\rangle$ states can be readily extracted from the Rabi precession at the corresponding nuclear transitions. The combined analysis of the selective electron and nuclear Rabi oscillations together with the known rotational symmetry and the normalization condition based on the Boltzmann state give enough freedom to determine all populations. These arguments also apply to the diagonal part of the pseudo-entangled states. The following diagonal elements for ρ_7 were obtained: $\{-0.01, 0.04, 0, 0.34, \frac{1}{2}, 0.16, 1, -0.03\}$

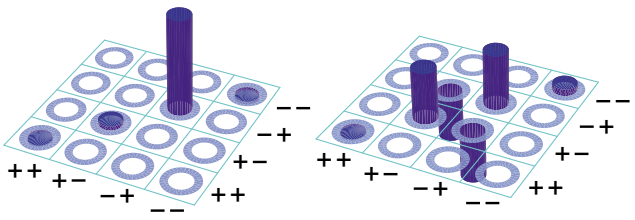

FIG. 2 (color online). Pictorial representation of the initial density matrix $\rho_{(-+)}$ (left) and the density matrix of the entangled state $\rho_{\Psi^{(-)}}$ (right) of the fictitious two-qubit sublevel states $|\pm\pm\rangle$ as defined in the text. For details on the values displayed see Eq. (5) and the corresponding text.

where the values $(0, \frac{1}{2}, 1)$ are residuals from the Boltzmann state and are unaffected by the preparation and the tomography sequences. Notice that the data set $\{-0.01, 0.04, 1, -0.03\}$ corresponds to the two-qubit subspace which is displayed in Fig. 2(left). The preparation of the pseudopure density matrix ρ_8 proceeds in a similar way as described for ρ_7 where instead of the $P_y^{(-)}(\beta_0)$ a $P_y^{(+)}(\beta_0)$ pulse is applied at the $m_I = +1/2$ sublevel system.

In analogy to the two-qubit Bell states we consider in the following the density matrices $\rho_{\Psi^{(\pm)}} = \frac{1}{2}|2 \pm 7\rangle\langle 2 \pm 7|$ and $\rho_{\Phi^{(\pm)}} = \frac{1}{2}|1 \pm 8\rangle\langle 1 \pm 8|$ as entangled states of this fictitious two-qubit subsystem. The preparation of $\rho_{\Psi^{(-)}}$ was performed by applying the unitary transformation $U_{\pm}^{(27)} = P_y^{(-)}(\mp\pi)P_y^{(78)}(\pi/2)$ to the initial density matrix $\rho_{(-+)}$. A density matrix tomography was also applied to this state. The corresponding data are presented pictorially in Fig. 2(right). The relevant part of the theoretically expected density matrix centers at the $\pm$ states with values of ± 0.5, and all other elements are expected to be zero. The experimental values deviate from this, of course, and can be obtained from the total density matrix given by Eq. (5). Note the negative sign of the off-diagonal elements, which is characteristic for the $\Psi^{(-)}$ state. In a similar way the other Bell states $\rho_{\Psi^{(+)}}$ and $\rho_{\Phi^{(\pm)}}$ were generated.

In order to identify the degree of entanglement and which entangled state was generated we have applied the density matrix tomography as described earlier [11] which is based among others on the characteristic phase dependence of the entangled states. In order to map out the phase characteristic of the entangled states we have applied phase rotations with angles (ϕ_1, ϕ_2) about the z axis of both spins by applying the detection sequence $U_{\rm d}^{(27)} = P_x^{(78)}(\pi/2, \phi_2)P_x^{(-)}(-\pi, \phi_1)$ for the tomography of the $\rho_{\Psi^{(\pm)}}$ states. The phase rotation angles ϕ_1 and ϕ_2 were varied independently. The fingerprint of entanglement is the intimately related phase dependence of the tomography signal which varies as $\cos(3\phi_1 - \phi_2)$ for the $\Psi^{\pm}$ states. Note the variation with $3\phi_1$ which results from the $\pm\frac{3}{2}$ quantum states of the electron spin involved in the entangled states considered here. Equivalently we apply

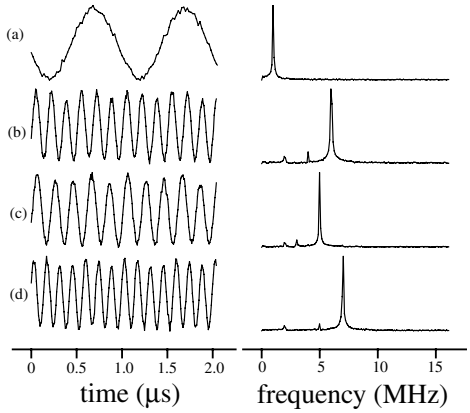

FIG. 3. Phase interferograms (left) and corresponding spectra (right) for the entangled states with phase incrementation frequencies $\nu_1 = 2.0$ MHz and $\nu_2 = 1.0$ MHz as discussed in the text. (a) $\nu_1 = 0$, $\nu_2 = 1.0$ MHz; (b) $3\nu_1 = 6.0$ MHz, $\nu_2 = 0$; (c) $3\nu_1 - \nu_2 = 5.0$ MHz as expected for $\rho_{\Psi^{(-)}}$; (d) $3\nu_1 + \nu_2 = 7.0$ MHz as expected for $\rho_{\Phi^{(+)}}$. See text for additional lines.

for the detection of the $\rho_{\Phi^{\pm}}$ states the unitary transformation $U_{\rm d}^{(18)} = P_x^{(78)}(\pi/2, \phi_2)P_x^{(+)}(-\pi, \phi_1)$ resulting in the detection signal proportional to $\cos(3\phi_1 + \phi_2)$.

Experimental results of this procedure applied to the entangled states $\rho_{\Psi^{(-)}}$ and $\rho_{\Phi^{(+)}}$ are shown in Fig. 3. When incrementing the phases of the detection sequence according to $\delta\phi_j = 2\pi\nu_j\delta t$ with $j \in (1, 2)$, an oscillatory phase evolution is expected as is, indeed, experimentally observed in Fig. 3. In Figs. 3(a) and 3(b) only one of the phases was incremented, whereas in Figs. 3(c) and 3(d) both phases were incremented. Note the specific phase variation of the entangled states Ψ [Fig. 3(c)] and Φ [Fig. 3(d)] in contrast to the single spin phase variations in Figs. 3(a) and 3(b). The corresponding spectra obtained after Fourier transformation of the phase evolutions show this even more clearly and are displayed in Fig. 3(right). We point at the typical signatures for the entangled states with lines appearing at frequencies $3\nu_1 \pm \nu_2$. The other weak lines are artifacts due to pulse imperfections. They also reflect the multilevel nature of our system which, in fact, allows in principle all of the following phase frequencies $\{\nu_1, 2\nu_1, 3\nu_1, \nu_2\}$ and $\{\nu_1 \pm \nu_2, 2\nu_1 \pm \nu_2 3\nu_1 \pm \nu_2\}$ to be observed. The fact is that basically only the expected $3\nu_1 \pm \nu_2$ are seen, whereas the other signals are small hints at the large fidelity of the prepared pseudoentangled states. The relative signal strength of the residual signals allows one to quantify the experimental errors. This has, in fact, been utilized in the tomography. A quantitative evaluation of the degree of entanglement results in the data shown in Fig. 2(right).

The difference of the system investigated here with respect to a pair of spins 1/2 relates to its multilevel nature such as is encountered in ionic and atomic systems as was mentioned in the introduction. In order to illustrate this, we present the full density matrix after tomography of $\rho_{\Psi^-}^{27}$ in Eq. (5).

$$\begin{pmatrix} -0.01 & \mathbf{0} & 0 & 0 & 0 & 0 & \mathbf{0} & \mathbf{0} \\ \mathbf{0} & 0.46 & 0 & 0.07 & 0 & 0.01 & -0.35 & \mathbf{0} \\ 0 & 0 & 0 & 0 & 0 & 0 & 0 & 0 \\ 0 & 0.07 & 0 & 0.18 & 0 & 0.04 & -0.11 & -0.01 \\ 0 & 0 & 0 & 0 & \frac{1}{2} & 0 & 0 & 0 \\ 0 & 0.01 & 0 & 0.04 & 0 & 0.31 & -0.01 & 0.06 \\ \mathbf{0} & -0.35 & 0 & -0.11 & 0 & -0.01 & 0.49 & \mathbf{0} \\ \mathbf{0} & \mathbf{0} & 0 & -0.01 & 0 & 0.06 & \mathbf{0} & 0.06 \end{pmatrix}. \quad (5)$$

The subspace corresponding to the Bell states as defined in Eq. (3) is marked in boldface and displayed in Fig. 2 after correction for decoherence. Experimental errors are on the order of ± 0.03 for the off-diagonal elements and ± 0.05 for the diagonal elements. Note that elements labeled 0 are unaffected by the preparation sequence, as is the element $\frac{1}{2}$. Both are residuals from the Boltzmann matrix. The off-diagonal elements $|27\rangle = |72\rangle$ were measured as -0.35 instead of the theoretically expected -0.5. This is due to the decoherence during the evolution between the creation and the detection of the entangled state with a measured decoherence time of 213 ns. Correcting for decoherence scales the off-diagonal value -0.35 up to -0.42 ± 0.04 which is displayed in Fig. 2. There are also pulse imperfections which lead to a deviation from the ideal values. Alternatively we were able to determine the pulse imperfections experimentally and calculated the expected entangled state which gave similar results. In a more extended publication we will address these and other aspects in more detail [21].

The density matrix we have been dealing with is *separable* and the entangled states we have prepared are properly called pseudoentangled states because of the temperature of 50 K applied here. However, when reaching a high electron spin polarization the experiments presented here can be shown to reach the quantum limit (see Warren *et al.* [17]). In order to estimate the characteristic temperature T_Q for reaching the quantum limit for the entangled states presented here, we applied the positive partial transpose criterion [22,23]. As a result we find the relation $\hbar\omega_S/k_B T_Q = \frac{1}{3}\log(3 + 2\sqrt{2})$, provided we apply initially a selective π pulse on one of the ESR hyperfine lines in order to create a spin aligned state out of the Boltzmann state. The corresponding quantum critical temperature is $T_Q = 7.76$ K for an ESR frequency of 95 GHz. Cooling below this temperature would convert the pseudoentangled states into quantum entangled states. Obviously this scenario is well in reach of current ESR installations.

In summary, we have shown that $^{15}N@C_{60}$ represents a multilevel system which can be reduced to a two-qubit subsystem by utilizing the appropriate electron and nuclear spin sublevels. We present here a novel approach to prepare and detect entangled states of an electron spin 3/2 with a nuclear spin 1/2. Moreover, we provide a calculation of the quantum limit for this system and the characteristic frequency or temperature where the pseudoentangled state crosses over to a quantum entangled state. These findings will provide further stimulus to ensemble quantum computing.

We acknowledge financial support by the Bundesminister for Bildung und Forschung (BMBF) and the Landesstiftung Baden-Wuerttemberg. We are grateful to J. Mende for discussions and experimental support.

[1] A. Einstein, B. Podolsky, and N. Rosen, Phys. Rev. **47**, 777 (1935).
[2] D. Deutsch, Proc. R. Soc. London A **400**, 97 (1985).
[3] J.-W. Pan, D. Bouwmeester, M. Daniell, H. Weinfurter, and A. Zeilinger, Nature (London) **403**, 515 (2000).
[4] J.-W. Pan, M. Daniell, S. Gasparoni, G. Weihs, and A. Zeilinger, Phys. Rev. Lett. **86**, 4435 (2001).
[5] C. A. Sacket *et al.*, Nature (London) **404**, 256 (2000).
[6] T. Almeida Murphy, T. Pawlik, A. Weidinger, M. Hoehne, R. Alcala, and J. M. Spaeth, Phys. Rev. Lett. **77**, 1075 (1996).
[7] N. Weiden, H. Käss, and K. P. Dinse, J. Phys. Chem. B **103**, 9826 (1999).
[8] W. Harneit, Phys. Rev. A **65**, 032322 (2002).
[9] D. Suter and K. Lim, Phys. Rev. A **65**, 052309 (2002).
[10] J. Twamley, Phys. Rev. A **67**, 052318 (2003).
[11] M. Mehring, J. Mende, and W. Scherer, Phys. Rev. Lett. **90**, 153001 (2003).
[12] D. G. Cory, A. F. Fahmy, and T. F. Havel, Proc. Natl. Acad. Sci. U.S.A. **94**, 1634 (1997).
[13] I. L. Chuang, L. M. K. Vandersypen, D. W. L. Xinlan Zhou, and S. Lloyd, Nature (London) **393**, 143 (1998).
[14] I. L. Chuang, N. Gershenfeld, and M. Kubinec, Phys. Rev. Lett. **80**, 3408 (1998).
[15] J. A. Jones and M. Mosca, J. Chem. Phys. **109**, 1648 (1998).
[16] R. Laflamme, E. Knill, W. H. Zurek, P. Catasti, and S. V. S. Mariappan, Philos. Trans. R. Soc. London A **356**, 1941 (1998).
[17] W. S. Warren, N. Gershenfeld, and I. Chuang, Science **277**, 1688 (1997).
[18] D. G. Cory, M. D. Price, and T. F. Havel, Physica (Amsterdam) **120D**, 82 (1998).
[19] N. A. Gershenfeld and I. L. Chuang, Science **275**, 350 (1997).
[20] E. Knill, I. Chuang, and R. Laflamme, Phys. Rev. A **57**, 3348 (1998).
[21] W. Scherer and M. Mehring (to be published).
[22] A. Peres, Phys. Rev. Lett. **77**, 1413 (1996).
[23] M. Horodecki, P. Horodecki, and R. Horodecki, Phys. Lett. A **223**, 1 (1996).